Martini straight

De Jong, Djurre H.; Baoukina, Svetlana; Ingólfsson, Helgi; Marrink, Siewert J.

Published in:
Computer Physics Communications

DOI:
10.1016/j.cpc.2015.09.014

Computer Physics Communications 199 (2016) 1–7

Contents lists available at ScienceDirect

Computer Physics Communications

journal homepage: www.elsevier.com/locate/cpc

Martini straight: Boosting performance using a shorter cutoff and GPUs

Djurre H. de Jong [a], Svetlana Baoukina [b], Helgi I. Ingólfsson [c], Siewert J. Marrink [c,*]

[a] Institut für Physikalische Chemie, Westfälische Wilhelms-Universität Münster, D-48149 Münster, Corrensstraße 30, Germany

[b] Department of Biological Sciences and Centre for Molecular Simulation, University of Calgary, Calgary, Alberta, Canada

[c] Groningen Biomolecular Sciences and Biotechnology Institute and Zernike Institute for Advanced Materials, University of Groningen, Nijenborgh 7, AG Groningen 9747, The Netherlands

ARTICLE INFO

Article history:
Received 15 July 2015
Received in revised form
18 September 2015
Accepted 21 September 2015
Available online 13 October 2015

Keywords:
Gromacs
Coarse-Grain
Verlet neighbor search
Lennard-Jones

ABSTRACT

In molecular dynamics simulations, sufficient sampling is of key importance and a continuous challenge in the field. The coarse grain Martini force field has been widely used to enhance sampling. In its original implementation, this force field applied a shifted Lennard-Jones potential for the non-bonded van der Waals interactions, to avoid problems related to a relatively short cutoff. Here we investigate the use of a straight cutoff Lennard-Jones potential with potential modifiers. Together with a Verlet neighbor search algorithm, the modified potential allows the use of GPUs to accelerate the computations in Gromacs. We find that this alternative potential has little influence on most of the properties studied, including partitioning free energies, bulk liquid properties and bilayer properties. At the same time, energy conservation is kept within reasonable bounds. We conclude that the newly proposed straight cutoff approach is a viable alternative to the standard shifted potentials used in Martini, offering significant speedup even in the absence of GPUs.

1. Introduction

One of the key challenges in the field of molecular dynamics (MD) simulations is to obtain sufficient sampling of the relevant phase space to justify the ergodicity principle, known as the sampling problem [1]. Several methods to increase the sampling are available, among which the use of designated hardware [2], distributed sampling [3], enhanced sampling methods [4] and the use of coarse grain (CG) models [5]. In the last category, the Martini model has become the most widely applied CG force field in the area of biomolecular simulations [6]. To reduce the effect of relatively short cutoffs, the Martini model [7,8] has been parameterized with the use of shifted functions for the non-bonded potentials. In their shifted form, an extra term is added to the Lennard-Jones (LJ) and Coulomb forces and potentials to assure continuity at the cutoff.

However, the formulation of a shifted potential is much more complex and computationally expensive compared to a pure LJ or Coulomb potential (although, in some MD-codes (e.g. Gromacs, the native MD-code for the Martini force field) the performance of shifted potentials is somewhat improved by tabulating the potentials at the start of every run [9]). Additionally, the implementation of shifted or switched potentials and forces differs in some of the major MD-codes [9,10], limiting the transferability of the Martini force field.

Substituting shifted potentials by straight cutoffs would simplify the implementation and increase transferability of the Martini model. In order to (better) conserve energy when potentials are being cutoff at a finite distance, potentials and/or forces can be modified. In recent versions of Gromacs this is implemented in the form of "*Potential modifiers*" and "*Force modifiers*". Specifically, potential modifiers shift the complete potential by a constant value so that it is zero at the cutoff. This has no influence on the force. This option is implemented for both van der Waals and Coulomb interactions. If additionally the forces have to be zero at the cutoff, one can use a reaction-field approach for Coulomb interactions. For van der Waals interactions force modifiers can be used: the forces can be switched to zero between a set distance and the cutoff, or the potential can be smoothly switched to zero between a set distance and the cutoff, thus yielding zero forces at the cutoff.

The development team of Gromacs is planning to depreciate the current implementation of shifted cutoffs, in favor of potential

* Corresponding author.
E-mail address: s.j.marrink@rug.nl (S.J. Marrink).

http://dx.doi.org/10.1016/j.cpc.2015.09.014
0010-4655/

and force modifiers. The newly introduced Verlet neighbor search (VNS) algorithm [11] already lacks support for the use of shifted potentials. In the current Gromacs versions, only VNS supports multi-level parallelization (OpenMP multithreading combined with MPI) and can be used for simulations on GPUs [12].

In the current work, we evaluate the performance of the Martini force field with straight cutoffs in combination with potential and force modifiers. To do so, we have selected a number of representative properties (that we believe are important for performance) of the Martini model. These include partitioning free energies, bulk water properties and lipid bilayer properties. In addition, we consider energy conservation for different systems. We compare the newly proposed cutoff scheme to the original Martini scheme, and its common variation providing better energy conservation [13].

2. Methods

2.1. Simulation parameters

For all measured properties we compared four sets of parameters.

(i) '*Old*': parameters as used in the original Martini paper. Specifically: a timestep of 40 fs, a neighbor list length of 1.2 nm with the neighbor list created using the 'group-scheme' every 10 steps and potentials and forces are shifted to zero using the Gromacs shifting function between 0.9–1.2 nm and 0.0–1.2 nm for Lennard-Jones (LJ) and Coulomb interactions, respectively. The Berendsen weak coupling scheme [14] was used with coupling parameters of 1.0 and 3.0 ps^{-1} for temperature and pressure, respectively.

(ii) '*Common*': parameters as they are commonly found in recent Martini papers. The timestep is reduced to 30 fs, and the neighbor list length is increased to 1.4 nm to allow for a diffusion buffer. In a recent comparison [13] these run parameters were found to give good energy conservation. Other parameters are the same as for '*Old*'.

(iii) '*New*': Parameters currently tested. A timestep of 30 fs is used. The neighbor list is updated using the Verlet neighbor search (VNS) algorithm, with the neighbor list length being automatically determined. LJ and Coulomb potentials and forces are cut off at 1.1 nm, with the potentials shifted to zero at the cut off using the "*Potential modifiers*" (see *Results*). The neighbor list is updated every 20 steps. Velocity rescale [15] and Parrinello–Rahman coupling schemes [16] are used with coupling parameters of 1.0 and 12.0 ps^{-1}.

(iv) '*New-RF*': the same as '*New*' except for the Coulomb interactions a reaction-field potential with $\varepsilon_{rf} = \infty$ is used.

For all three sets a leapfrog integrator is used, unless stated otherwise. The temperature and pressure are kept constant at 298.15 K and 1 bar, respectively. Unless stated otherwise Version 4.6.3 or 4.6.6 of the Gromacs software package was used [9,12].

2.2. Free energies of vaporization, hydration and solvation

For the 18 Martini bead types free energies of vaporization, hydration and solvation in ether, chloroform, hexadecane and octanol are determined. The systems contain 3199 (vaporization, hydration and solvation in ether, chloroform), 800 (solvation in hexadecane) or 536 (solvation in octanol) molecules. The octanol additionally contains 48 water beads to create a saturated solution. Free energies are obtained using free energy perturbation (FEP), by stepwise turning of the interactions between a solute bead and the solvent following a parameter λ. The interactions are turned of in 21 steps ('windows'). "Soft core" potentials were used in order to avoid high energies due to overlapping particles. Soft core parameters α, σ and *power* were set to 1.3, 0.47 nm and 1, respectively. For every window 25,000 steps are performed, of which the first 100 ps are discarded as equilibration. At every window the $\Delta G/\Delta\lambda$ is calculated for the current lambda value and the lambda value of the neighboring windows. Afterwards total free energies are calculated using Bennet's Acceptance Ratio (BAR) implemented in the Gromacs utility g_bar [9].

2.3. Surface tension

Surface tensions are calculated for three systems (water–hexadecane, water–air, and hexadecane–air) and two system sizes. The small system consisted of 400 beads per solvent phase, the large system of 1600 beads per solvent phase. Simulations were run for 1 μs each at a temperature of 293 K. The surface tension was calculated using $g = 1/2 * L(\langle P_z - P_{\|}\rangle)$, where L is the box length, P_z and $P_{\|}$ are the pressure components perpendicular and parallel to the surface respectively and the angular brackets indicate time averaging.

2.4. Energy conservation

Energy conservation was studied by simulating a box of 3200 Martini water beads or 800 hexadecane molecules for 1.2 ns in a NVE and NpT ensemble. Energies were saved every timestep. Analyses were performed over the last 600 ps using the Gromacs tool g_energy. For the simulations in the NVE ensemble we calculated the average temperature and the drift in total energy divided by the drift in potential energy. For the NpT simulations we calculated the average temperature, the average potential energy and the squared temperature scaling factor, λ. The latter gives the average scaling of the particle velocities, e.g. a value larger than one means the thermostat adds energy to the system and vice versa.

2.5. Bulk water properties

A cubic system containing 3200 water beads (1600 for the polarizable water system [17]) was relaxed and subsequently simulated under NpT conditions for 0.24 and 16 ns, respectively. The same system was used to calculate the isothermal compressibility, κ_T, where the volume was reduced and increased by 1% compared to the equilibrium volume of the density simulation. The compressibility was calculated using $\kappa_T = (V_1 - V_2)/(V(p_2 - p_1))$, where V_x and p_x are the volume and pressure of the system that are 1% enlarged (1) or reduced (2) and V is the equilibrium volume. Note that for polarizable water, due to numerical stability issues the timesteps had to be reduced to 30, 20 and 20 fs for the '*Old*', '*Common*' and '*New*' parameter sets, respectively.

2.6. Bilayer properties

Lipid bilayers of two sizes were simulated in explicit water and with counter ions where appropriate. Fully hydrated small symmetric bilayers of 242 lipids each were created using the *insane.py* [18] script (available at www.cgmartini.nl). The same 100 different diacylglycerol lipid types were simulated as described in [18]. Each bilayer was simulated for 1 μs at 310 K. Five different lipid headgroups were modeled: phosphatidylcholines (PC), phosphatidylethanolamine (PE), phosphoglycerol (PG), phosphatidylserine (PS), and phosphatidic acid (PA) lipids. Each headgroup was combined with 20 different tails, corresponding to atomistic tails ranging from 6 to 24 carbon atoms and from fully saturated to polyunsaturated. Note, the PA lipids used were protonated (−1 net charge) as pure mixtures of unprotonated Martini PA lipids (−2 net charge) do not form stable bilayers.

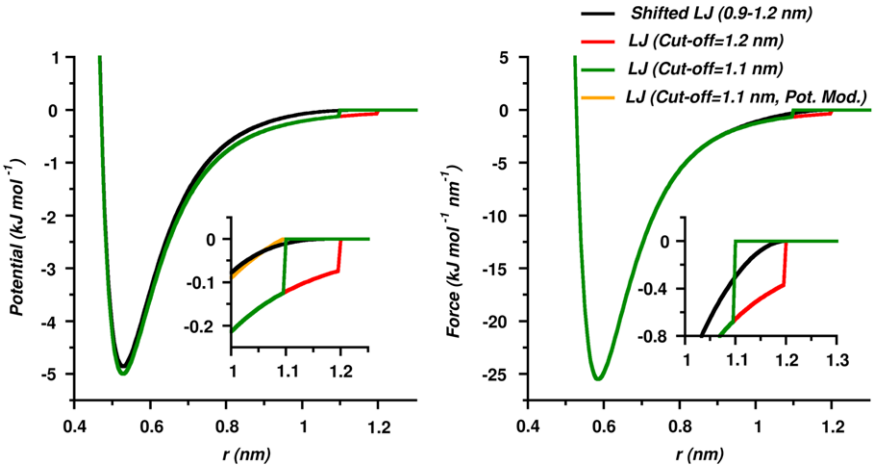

Fig. 1. Plot of potential energy and force of a Lennard-Jones function with $\varepsilon = 5.0$ kJ/mol and $\sigma = 0.47$ nm. Shown are the LJ potential shifted between 0.9 and 1.2 nm used by Martini (black lines) and pure LJ functions cutoff at 1.1 and 1.2 (red and green lines). The Lennard-Jones potential with "*Potential modifier*" largely falls behind the black line, but is visible in the inset of the left panel (orange line). (For interpretation of the references to color in this figure legend, the reader is referred to the web version of this article.)

A larger bilayer of 4608 dipalmitoylphosphatidylcholine (DPPC) lipids and 128,000 CG water beads was simulated for 1.2 μs at three different temperatures (280, 290 and 323 K), to compare the bilayer properties in the liquid-crystalline and gel phases. The hydration level was increased for the larger systems to accommodate thermal undulations. Additionally, a larger bilayer of 4608 dilineoylphosphatidylcholine (DLiPC; called DIPC in Martini) was simulated at 300 K, to compare the effects of the cutoff parameters for unsaturated lipids.

The different lipid properties were calculated as follows. The area per lipid, A_L, is calculated as $(\langle L_x\rangle \langle L_y\rangle)/N$, where L is the lateral box dimension in x and y dimension, angular brackets indicate the time average, and N is the number of lipids per monolayer. The bilayer thickness is measured as the distance between the maxima of the PO_4-bead densities along the z-axis. The bilayer area compressibility modulus, K_A, is calculated as $kT\langle A\rangle/(N\langle(A-A_0)^2\rangle)$, where kT is the Boltzmann constant and temperature in Kelvin, A the box area and A_0 the equilibrium box area. The lipid tail order parameter, P_2, is calculated as $1/2(3\langle\cos^2(\theta)\rangle - 1)$, where θ is the angle between the normal of the bilayer surface (approximated using the box z-axes) and the vector along each bond in the lipid tails. The lipid lateral diffusion is calculated using the mean square displacement (MSD) of the PO_4-beads obtained with the g_msd tool in Gromacs.

2.7. Speedup

The speedup is measured using the smaller and larger DPPC bilayer systems described in the above sections. The smaller systems were simulated for 30 min, with the cycle counters reset halfway (-resethway), and no structure, energy, log or state files or final configuration was written out (-noconfout). All systems ran for at least 50,000 steps. The larger DPPC bilayers were simulated at 323 K for 50,000 steps; the performance of '*Common*' and '*New*' cutoff parameters was compared.

3. Results

3.1. New non-bonded LJ potential

In the standard Martini model, the Gromacs shift function is used to have both the LJ potential and force vanish at the cutoff. The intended use of a straight cutoff in the current implementation implies (re)introducing artifacts arising from the discontinuities in potential and force when particle pairs cross the cutoff distance (cf. Fig. 1). A logical choice when trying to avoid cutoff artifacts is the use a longer cutoff distance. This way the potential will be close to zero at the cutoff. For example, at a cutoff of 3σ, the error is reduced to 0.005ε, compared to 0.014ε for the cutoff distance used in the Martini model ($1.2\text{ nm} = 2.55\sigma$). However, both the longer cutoff and use of a non-shifted potential would make the potential more attractive, thus disturbing the balance between different interactions in the model.

To restore the balance while avoiding a complete reparametrization of the Martini force field we investigated the use of a shorter cutoff ($1.1\text{ nm} = 2.34\sigma$), in combination with potential modifiers. Without potential modifiers, the potential at the cutoff is still 0.024ε. The modifiers shift the complete potential up by the difference at the cutoff, thus effectively creating a potential that is zero at the cutoff. Comparing the new potential to the standard Martini potential, the overall shape is maintained (Fig. 1). However, a significant discontinuity in the force remains. In the remainder we investigate how well this potential reproduces results with the normal Martini potential and what the influence of the discontinuity at the cutoff is on energy conservation.

For the non-bonded Coulomb potential, a straight cut-off was compared to using a reaction-field (Fig. 2). Since Coulomb interactions are much longer ranged, artifacts at the cutoff are expected to be much larger. This can be corrected by using a reaction-field approach where the potential is smoothly changed to zero at the cutoff by assuming a fixed dielectric constant beyond the cutoff. [19] Note however, that Martini systems are very sparsely charged: most systems tested in this work are neutral and for a lipid bilayer system the total Coulomb energy is typically around 1% of the total LJ energy. The local charge density might however be much higher and charges could significantly affect system properties.

3.2. Free energies

One of the corner stones of the Martini force field is the reproduction of experimental partitioning free energies. A crucial test for the new non-bonded scheme is therefore to assess whether or not free energies remain unchanged. Free energies of vaporization, hydration and solvation in ether, chloroform, hexadecane, and octanol have been calculated for all 18 Martini beads and for each of the three sets of parameters. The full list of free energies can be found in the supplementary information (Tables S1, S2, S3, S4, S5 and S6).

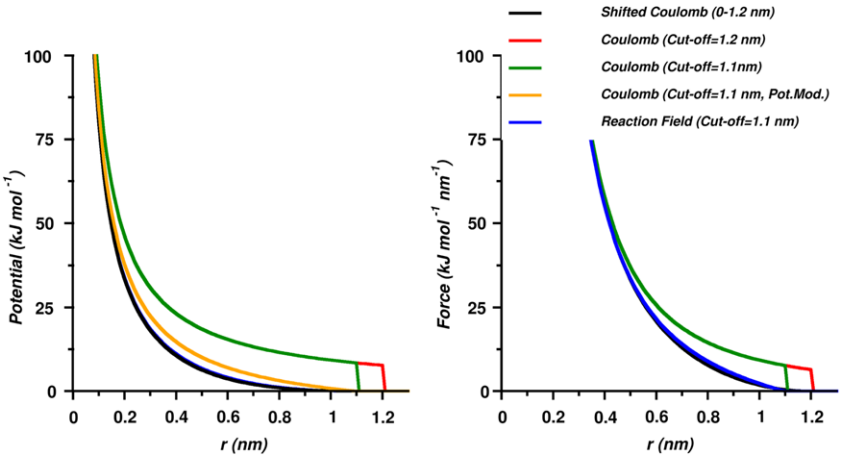

Fig. 2. Plot of potential energy and force of a Coulomb function for two equal elementary charges. Shown are the Coulomb potential shifted between 0 and 1.2 nm used by Martini (black lines), the pure Coulomb functions cutoff at 1.1 and 1.2 (red and green lines), the pure Coulomb potential with a "*Potential modifier*" (orange line) and the reaction-field potential with $\varepsilon_{rf} = \infty$ (blue line). $\varepsilon = 15.0$ for all potentials. (For interpretation of the references to color in this figure legend, the reader is referred to the web version of this article.)

Table 1
Comparison of the combined data for solvation, hydration and partitioning free energy. Data obtained for the three sets of run parameters ('*Old*', '*Common*' and '*New*') are mutually compared and additionally compared the values previously published [8]. Values given are the number of data points, the Pearsons correlation coefficient, *R*, and the Root Mean Square Difference (RMSD). Data points where no value was obtained (e.g. because the system was solid) or where only a lower bound was obtained are omitted in the comparisons.

	'*Old*' vs. '*Common*'	'*Old*' vs. '*New*'	'*Common*' vs. '*New*'	'*Published*' vs. '*Old*'	'*Published*' vs. '*Common*'	'*Published*' vs. '*New*'
Data points	104	104	104	99[a]	99[a]	99[a]
R	0.9990	0.9992	0.9989	0.9925	0.9913	0.9919
RMSD (kJ/mol)	0.7574	0.7505	0.9359	1.7383	1.7758	1.9504

[a] The number of data points is lower since in the original publication no (exact) values were given for the vaporization free energy of the P5 bead and water–hexadecane partitioning free energies of the charged particles.

Table 2
Density and isothermal compressibility of bulk water.
Source: Experimental values are taken from [20].

	'*Old*'	'*Common*'	'*New*'	'*New-RF*'	'*Published*'	*Exp.*
Density (g/dm^3) $\pm$ SE	1004.4 $\pm$ 0.01	1002.2 $\pm$ 0.03	1008.2 $\pm$ 0.04		0.99 $\times$ 10^3	996
Density (polarizable water) (g/dm^3) $\pm$ SE	1044.2 $\pm$ 0.01	1043.9 $\pm$ 0.03	1048.4 $\pm$ 0.11	1048.3 $\pm$ 0.06	1043	996
Compressibility ($\times 10^{-5}$ bar^{-1}) $\pm$ SE	8.4 $\pm$ 0.03	8.5 $\pm$ 0.03	8.2 $\pm$ 0.04		6.0	4.5

Table 1 lists the Pearson correlation coefficients and RMSD averaged over all of the free energies compared between the three parameter sets and values previously published [8]. The correlation coefficients between all sets are high (>0.99) and the RMSDs are within 1 kJ/mol for the free energies calculated in this work. The larger difference between the values calculated in the current work and those published earlier is probably due to the use of a different method to calculate the free energies (counting particles in the previous work, versus BAR here).

3.3. Bulk water properties

To evaluate the effect of the new straight cutoff scheme on bulk water properties, we calculated the density, and compressibility of a box of CG water particles. Both normal Martini water, and the polarizable Martini water were considered. Results are shown in Table 2 for the three parameter sets. The density of water is slightly higher than the experimental value for all three parameter sets. The values for the '*Old*' and '*Common*' sets are similar, while the '*New*' value is slightly higher. A similar trend is seen for the polarizable water. The calculated compressibilities are also very similar between the three methods. The current value is considerably higher than the previously published value, which was obtained using a different method based upon the fluctuations in an NpT-ensemble.

Table 3
Comparison of interfacial surface tension. Reported values are in mN/m. For every system the two values are those obtained for a small and a large system. The 'Published' values are those reported in the Martini paper [7]. Error of the order of 1 mN/m.
Source: Experimental data (Exp.) are taken from [20,21].

	'*Old*'	'*Common*'	'*New*'	'*Published*'	Exp.
Water/vapor	34/33	33/33	35/34	45/30	73
Dodecane/vapor	24/24	24/24	25/25	25/23	24
Water/dodecane	43/43	43/42	44/43	70/50	52

3.4. Interfacial surface tension

Results for interfaces are shown in Table 3, reporting on the surface tension for water/vapor, dodecane/vapor, and water/dodecane systems. We find the surface tension to be consistent between all three sets of parameters. The differences between the values obtained in this work and those previously published, however, are relatively large; in contrast to the previous work we do not find a (strong) influence of system size on surface tension. To investigate this further, we simulated different sizes and geometries of the water/dodecane system, both with and without antifreeze particles (LJ particles with 10% larger sigma). The results are shown in Figure S1. As can be seen, the surface tension does not depend on the system size nor on the addition of anti-freeze particles.

Table 4
Energy conservation. Results are obtained from two simulations, one in the NVE ensemble, one in the NpT ensemble.

Parameter set	*Water*			*Hexadecane*		
	'*Old*'	'*Common*'	'*New*'	'*Old*'	'*Common*'	'*New*'
NVE: drift in T (K)	−46.2[a]	0.2	0.3	−150.2[b]	0.4	0.0
NVE: $\Delta E^{\text{tot}}/\Delta E^{\text{pot}}$	1.3	0.07	0.12	1.6	0.05	0.07
NpT: $\langle T \rangle$ (K)	298.9	299.9	300.2	298.8	299.9	300.2
NpT: $\langle E^{\text{pot}} \rangle$ (kJ mol^{-1})	−85 531	−85 367	−86 929	−47 345	−47 241	−48 259
NpT: $\langle \lambda^2 \rangle$	1.00016	1.00000	0.99998	1.00018	1.00000	1.00000

[a] System freezes.
[b] Vacuum bubble occurs.

3.5. Energy conservation

The use of a cutoff is prone to lead to poor energy conservation, resulting in possible heating or cooling of the system. To study energy conservation, we simulated water and hexadecane systems in both an NVE and an NpT ensemble. The drift in the simulation temperature, the average fluctuations in total energy divided by the average fluctuations in potential energy (NVE), the average potential energy and the temperature scaling factor, λ (NpT) were measured. Energy conservation of standard Martini was studied in a similar way [13]. The results are shown in Table 4.

We observe that the '*New*' parameter set gives (much) better energy conservation than the '*Old*' set and comparable to the '*Common*' set. The drift in temperature is small in NVE system for both water and hexadecane, while the heat flow in the NpT-simulations, measured by $\langle \lambda^2 \rangle$, is very close to one. The average potential energy for both systems in the NpT ensemble is higher with the '*New*' parameters compared to both other sets, indicative for the slightly higher density, as observed before.

We also calculated the energy conservation for polarizable water (Table S7). Both the '*New*' and the '*New-RF*' parameters sets give good energy conservation, comparable to the '*Common*'-set and much better than the '*Old*' parameters.

3.6. Bilayer properties

To assess the effects of the cutoff scheme for a more complex system, we simulated 100 different lipids types with the '*Common*', '*New*' and '*New-RF*' parameter sets.

For all the different lipid types and the '*Common*', '*New*' and '*New-RF*' parameter sets, five lipid properties were calculated: area per lipid, in-plane compressibility, average tail order parameter, lipid lateral diffusion and bilayer thickness. Comparison of the area per lipid for the '*Common*' and '*New*' parameters is shown in Fig. 3. Comparisons of the other lipid properties and '*Common*' vs. '*New-RF*' are shown in Figures S2 and S3, respectively, and all the bilayer properties calculated with error estimates are listed in Table S8. Overall lipid properties calculated using the '*Common*', '*New*' and '*New-RF*' parameter sets demonstrate an excellent agreement, see Fig. 3, S2, and S3, and at the CG level of representation can be said to capture the same lipid properties.

The properties of larger bilayers are shown in Table 5. The differences in area per lipid are small for all cases. These minor differences could lead to different phase behavior of DPPC bilayers close the main phase transition temperature (∼295 K in the Martini model).

Simulations of larger bilayers frequently crashed with the '*Old*' parameter set; besides, artificial box oscillations coupled to bilayer bending were observed in some cases (DLiPC bilayer). This problem was solved by reducing the time step to 0.03 ps. With the '*New*' parameters, the Parrinello–Rahman barostat gave rise to stronger area fluctuations. This led to problems with domain decomposition and caused simulations to crash. The magnitude of area fluctuations in *NpT* simulations is determined by both the coupling parameter, "τ_p", and "compressibility" parameters of the barostat. Increasing τ_p to 24 ps^{-1} or reducing compressibility to 5×10^{-6} provided stable simulations with domain decomposition for the '*New*' parameters.

For bilayer simulations using the polarizable Martini water model Coulomb interactions play a larger role. We compared the '*Common*', '*New*' and '*New-RF*' parameters sets for four different lipid types (DPPC, DOPC, DPPG and DOPG) using the small bilayer setup and a time step of 20 fs and $\varepsilon = 2.5$. Overall lipid properties showed a significant difference between the '*Common*' and '*New*'

Table 5
The area per lipid of larger bilayers (4608 lipids) at different temperatures.

Parameters	Lipid	T (K)	A_L (nm^2)	Phase
'*Old*'			0.461	Gel
'*Common*'	DPPC	280	0.460	Gel
'*New*'			0.459	Gel
'*Old*'			0.588	Liquid
'*Common*'	DPPC	290	0.575	Liquid
'*New*'			0.478	Gel
'*Old*'			0.636	Liquid
'*Common*'	DPPC	323	0.628	Liquid
'*New*'			0.630	Liquid
'*New-RF*'			0.626	Liquid
'*Old*'			0.737	Liquid
'*Common*'	DLiPC	300	0.737	Liquid
'*New*'			0.740	Liquid
'*New-RF*'			0.737	Liquid

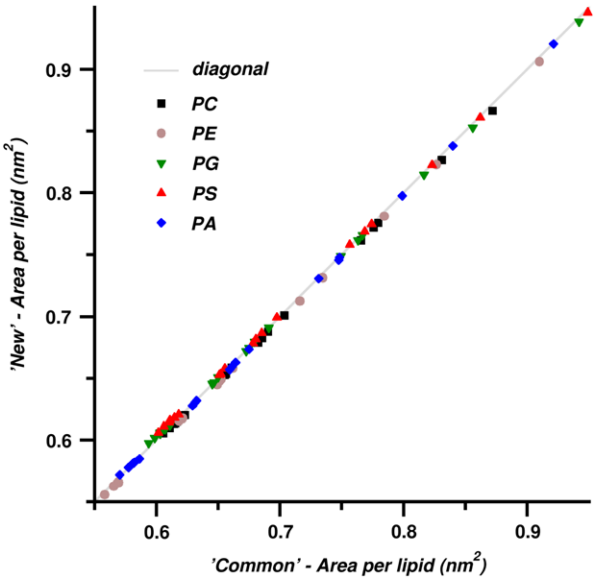

Fig. 3. Correlation of the area per lipid. Showing a comparison of area per lipid for 100 different Martini diacylglycerol lipid types for the '*Common*' and '*New*' parameter sets. A diagonal line is shown for reference in gray. A linear fit of the data gives a slope of 0.99 with R and RMSD > 0.999.

Table 6
Performance for a small DPPC bilayer (7568 CG beads) using different parameter sets.

Performance, ns/day	'*Old*'	'*Common*'	'*New*'	*New-RF*
1 core/CPU[a]	825	443	1 103	1 112
1 node × 12 cores[b]	5 264	2845	4 917[d]	4 855
4 nodes × 12 cores[b]	14 926	8586	14 098	13 410
1 node × 16 cores + 2 GPUs[c]	4 647	2483	4 524[e]	4 506[e]

[a] Intel I7-3770, 3.4 GHz.
[b] Intel Xeon-E5504, 2.0 GHz.
[c] AMD Opteron-6134, 2.3 GHz and NVIDIA Tesla C2070 GPUs.
[d] 2 OMP-processes per MPI-process.
[e] 8 OMP-processes per MPI-process.

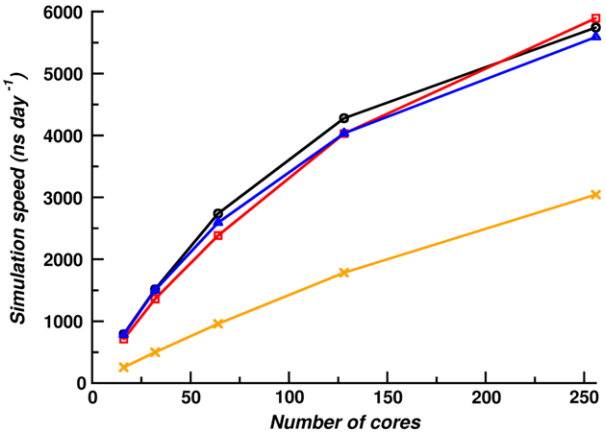

Fig. 4. Performance for a large DPPC bilayer (183,296 CG beads) with the '*Common*' (Orange line), '*New*' (Black line) and '*New-RF*' (*Blue line*) with Gromacs v.4.6.7 and 'New-5' (Red line) with Gromacs v.5.0.2. Systems were simulated on Intel Xeon E5-2670, 2.6 GHz, NVIDIA Tesla K20, 16 CPUs + 2 GPUs per node; 2MPI processes per node, and 8 OMP threads per MPI-process were used. (For interpretation of the references to color in this figure legend, the reader is referred to the web version of this article.)

parameters sets but a fairly good agreement between '*Common*' and '*New-RF*', see Table S8.

3.7. Speedup

To assess the performance of the three parameter sets, we performed benchmarks for the small and large DPPC bilayers. It is important to note, that performance of a certain system depends on the specific hardware setup. Table 6 shows the performance on several platforms for a small DPPC bilayer (7568 CG beads). On a single core, where no domain decomposition is needed, both the '*Old*' and '*New*' parameter sets outperform the '*Common*' parameter set. For the '*Old*' set, this is partly due to the larger time step and partly due to the smaller neighbor search radius used. For the '*New*' parameter set it is due to the use of a pure LJ potential, shorter cutoff and VNS algorithm.

With increasing the number of CPUs, the '*Old*' and '*New*' parameter sets still give a large speedup compared to '*Common*' parameters. However, here having a smaller neighbor list becomes advantageous (less communication), thus the '*Old*' parameter outperforms the '*New*' parameters. Multi-level (hybrid) parallelization using a combination of MPI and OpenMP threads additionally improves performance, which increases significantly when using a large number of compute nodes with GPUs.

Additionally, we tested the speedup when using "*Force modifiers*" in Gromacs 5.0.2 by simulating the small and large DPPC bilayers (Table 7, Fig. 4). These effectively modify the forces in the same way as the shift function in older Gromacs codes. The '*New-5*'-parameter set is identical to the '*New*'-set, except "*Force modifiers*" are used instead of the "*Potential modifiers*", and the cut-offs are reset to 1.2 nm. Additional code optimizations in Gromacs 5 make a direct comparison of the simulation speed obtained with both Gromacs versions impossible. For the '*Old*', '*Common*' and '*New*' parameter sets, the trend is the same as in Table 6. The '*New-5*' simulations are considerably faster than with the '*Common*'-set, but not as fast as with the '*New*' parameters due to the shorter cutoff in the latter. On a GPU equipped cluster this disadvantage is diminished and the scaling to larger number of cores follows the same trend for all three parameter sets (Fig. 4).

Table 7
Performance in ns/day for a 256 DPPC lipids bilayer solvated in 4496 water beads using Gromacs 5 with the different parameter sets. 'A': Single core, Intel I7-3770 running at 3.4 GHz 'B': Eight core, Intel I7-3770 running at 3.4 GHz.

System	'*Old*'	'*Common*'	'*New*'	'*New-RF*'	'*New-5*'
'A'	814	448	1096	1103	820
'B'	4150	2319	4060	4062	2987

4. Conclusions

We have tested the Martini force field with four sets of run parameters: a straight Lennard-Jones and Coulomb cutoff ('*New*'), replacing the Coulomb cutoff with reaction-field ('*New-RF*'), using a shifted potential with commonly used cutoffs ('*Common*') and using a shifted potential with the original Martini model parameters ('*Old*').

We find that a significant speedup can be obtained by using the '*New*' or '*New-RF*' parameters as compared to the '*Common*' parameters, while proper energy conservation is retained. This in contrast to the '*Old*' parameter set, which gives a similar performance increase, but at the cost of worse energy conservation. Importantly, for the systems tested in this work the use of a straight LJ-cutoff did not affect system properties. Changes in, e.g., partitioning free energies are small and remain well within the margins given by differences between the Martini force field and experimental values. For charged systems using a reaction field to treat the Coulomb interactions gives slightly better results at negligible extra computational cost and is thus advisable. Using a straight cutoff also gives faster simulations in comparison to simulations using the "*Force modifiers*" in Gromacs 5, although this advantage is much smaller.

We conclude that the newly proposed cutoff scheme '*New-RF*' appears most suitable for simulations with the Martini force field, and can lead to a significant speedup while keeping energy conservation within reasonable bounds. In particular, the new scheme can be used to more easily implement Martini in other MD packages and to harness the power of GPUs. However, to assure wider applicability, additional testing on specific systems of interest is still recommended.

Acknowledgment

Berk Hess is acknowledged for stimulating discussions. DHdJ would like to acknowledge financial support from the Alexander von Humboldt Foundation.

Appendix A. Supplementary data

Supplementary material related to this article can be found online at http://dx.doi.org/10.1016/j.cpc.2015.09.014.

References

[1] W.F. van Gunsteren, D. Bakowies, R. Baron, I. Chandrasekhar, M. Christen, X. Daura, P. Gee, D.P. Geerke, A. Glättli, P.H. Hünenberger, M.A. Kastenholz, C. Oostenbrink, M. Schenk, D. Trzesniak, N.F.A. van der Vegt, H.B. Yu, Biomolecular modeling: Goals, problems, perspectives, Angew. Chem. Int. Ed. 45 (2006) 4064–4092.

[2] D.E. Shaw, R.O. Dror, J.K. Salmon, J.P. Grossman, K.M. Mackenzie, J.A. Bank, C. Young, M.M. Deneroff, B. Batson, K.J. Bowers, E. Chow, M.P. Eastwood, D.J. Ierardi, J.L. Klepeis, J.S. Kuskin, R.H. Larson, K. Lindorff-Larsen, P. Maragakis, M.A. Moraes, S. Piana, Y. Shan, B. Towles, Millisecond-scale molecular dynamics simulations on anton, in: P. Int. C. High Perform., SC09, 2009, pp. 1–11.

[3] M. Shirts, V.S. Pande, Screen savers of the world unite!, Science 290 (2006) 1903–1904.

[4] C. Abrams, G. Bussi, Enhanced sampling in molecular dynamics using metadynamics, replica-exchange, and temperature-acceleration, Entropy 16 (2014) 163–199.

[5] H.I. Ingólfsson, C.A. Lopez, J.J. Uusitalo, D.H. de Jong, S.M. Gopal, X. Periole, S.J. Marrink, The power of coarse graining in biomolecular simulations, WIREs Comput. Mol. Sci. 4 (2014) 225–248.

[6] S.J. Marrink, D.P. Tieleman, Perspective on the martini model, Chem. Soc. Rev. 42 (2013) 6801–6822.

[7] S.J. Marrink, A.H. de Vries, A.E. Mark, Coarse grained model for semiquantitative lipid simulations, J. Phys. Chem. B 108 (2004) 750–760.

[8] S.J. Marrink, H.J. Risselada, S. Yefimov, D.P. Tieleman, A.H. de Vries, The Martini force field: Coarse grained model for biomolecular simulations, J. Phys. Chem. B 111 (2007) 7812–7824.

[9] D. van der Spoel, E. Lindahl, B. Hess, the GROMACS development team, GROMACS User Manual version 4.6.4, 2013. http://www.gromacs.org.

[10] M. Bhandarkar, A. Bhatele, E. Bohm, R. Brunner, F. Buelens, C. Chipot, A. Dalke, S. Dixit, G. Fiorin, P. Freddolino, P. Grayson, J. Gullingsrud, A. Gursoy, D. Hardy, C. Harrison, J. Hénin, W. Humphrey, D. Hurwitz, N. Krawetz, S. Kumar, D. Kunzman, J. Lai, C. Lee, R. McGreevy, C. Mei, M. Nelson, J. Phillips, O. Sarood, A. Shinozaki, D. Tanner, D. Wells, G. Zheng, F. Zhu, NAMD User's Guide. https://www.s.ks.uiuc.edu/Research/namd/2.9/ug/.

[11] L. Verlet, Computer "Experiments" on classical fluids. I. Thermodynamical properties of Lennard-Jones molecules, Phys. Rev. 159 (1967) 98–103.

[12] S. Pronk, S. Páll, R. Schulz, P. Larsson, P. Bjelkmar, R. Apostolov, M.R. Shirts, J.C. Smith, P.M. Kasson, D. van der Spoel, B. Hess, E. Lindahl, Gromacs 4.5: a high-throughput and highly parallel open source molecular simulation toolkit, Bioinformatics 29 (2013) 845–854.

[13] S.J. Marrink, X. Periole, D.P. Tieleman, A.H. de Vries, Comment on using a too large integration time step in molecular dynamics simulations of coarse–grained molecular models, Phys. Chem. Chem. Phys. 12 (2010) 2254–2256.

[14] H.J.C. Berendsen, J.P.M. Postma, W.F. van Gunsteren, A. DiNola, J.R. Haak, Molecular dynamics with coupling to an external bath, J. Chem. Phys. 81 (1984) 3684–3690.

[15] G. Bussi, D. Donadio, M. Parrinello, Canonical sampling through velocity rescaling, J. Chem. Phys. 126 (2007) 014101.

[16] M. Parrinello, A. Rahman, Polymorphic transitions in single crystals: a new molecular dynamics method, J. Appl. Phys. 52 (1981) 7182–7190.

[17] S.O. Yesylevskyy, L.V. Schäfer, D. Sengupta, S.J. Marrink, Polarizable water model for the coarse-grained martini force field, PLOS Comp. Biol. 6 (2010) e1000810.

[18] T.A. Wassenaar, H.I. Ingólfsson, R.A. Böckmann, D.P. Tieleman, S.J. Marrink, Computational lipidomics with insane: a versatile tool for generating custom membranes for molecular simulations, J. Chem. Theory Comput. 11 (2015) 2144–2155.

[19] G. Tironi, R. Sperb, P.E. Smith, W.F. van Gunsteren, A generalized reaction field method for molecular dynamics simulations, J. Chem. Phys. 102 (1995) 5451–5459.

[20] D.R. Lide, CRC Handbook of Chemistry and Physics, seventy two ed., CRC Press, Boca Raton, FL, 1992.

[21] J. Amaya, D. Rana, V. Hornof, Dynamic interfacial tension behavior of water/oil systems containing in situ-formed surfactants, J. Solution Chem. 31 (2002) 139–148.